

Supporting information

Mechanistic Understanding of the Interactions Between Nano-Objects, with Different Surface Properties, and α -Synuclein

Hossein Mohammad-Beigi[†], Atiyeh Hosseini^{‡§}, Mohsen Adeli^{⊥¶}, Mohammad Reza Eftehadi^{||#*}, Gunna Christiansen[¶], Cagla Sahin^{‡□}, Zhaoxu Tu[¶], Mahdi Tavakol[■], Arezou Dilmaghani-Marand[°], Iraj Nabipour[●], Farshad Farzadfar[°], Daniel Erik Otzen^{†△*}, Morteza Mahmoudi^{▲*} and Mohammad Javad Hajipour^{°●*}

[†] Interdisciplinary Nanoscience Centre (iNANO), Aarhus University, Gustav Wieds Vej 14, DK – 8000 Aarhus C, Denmark.

[‡] Institute for Nanoscience and Nanotechnology (INST), Sharif University of Technology

[§] Center of Excellence in Complex Systems and Condensed Matter (CSCM), Sharif University of Technology, Tehran, 1458889694, Iran.

[⊥] Faculty of Science, Lorestan University, Khorramabad, Iran.

[¶] Department of Biology, Chemistry, Pharmacy, Institute of Chemistry and Biochemistry, Freie University Berlin, 14195 Berlin, Germany.

^{||} School of Nano Science, Institute for Research in Fundamental Sciences (IPM), P. O. Box 19395-5531, Tehran, Iran

[#] Department of Physics, Sharif University of Technology, Tehran, P. O. Box 11155-9161, Iran

[¶] Department of Biomedicine-Medical Microbiology and Immunology, Aarhus University, 8000 Aarhus C, Denmark.

[□] Science for Life Laboratory, Department of Microbiology, Tumor and Cell Biology, Karolinska Institutet, Solnavägen 9, 171 65 Stockholm, Sweden

[■] Department of Mechanical Engineering, Sharif University of Technology, Tehran, Iran

[°] Non-Communicable Diseases Research Center, Endocrinology and Metabolism Population Sciences Institute, Tehran University of Medical Sciences, Tehran, Iran.

● Persian Gulf Marine Biotechnology Research Center, The Persian Gulf Biomedical Sciences Research Institute, Bushehr University of Medical Sciences, Bushehr, Iran.

△ Department of Molecular Biology and Genetics, Aarhus University, Gustav Wieds Vej 14, DK – 8000 Aarhus C, Denmark.

▲ Department of Anesthesiology, Brigham and Women's Hospital, Harvard Medical School, Boston, Massachusetts, 02115, United States.

* Corresponding Authors: (MRE) e-mail: ejtehadi@sharif.edu; (DEO) e-mail: dao@inano.au.dk; (MM) e-mail: mmahmoudi@bwh.harvard.edu; (MJH) e-mail: mj.hajipour@ncdrc.info

Molecular dynamic simulation

The results of molecular dynamic simulation analyses indicate that a primary driving force for initiating the interactions between graphene⁽⁺⁾ and α -syn is electrostatic attraction, like the interactions among three α -syn monomers, as mentioned in the main text. After 20 ns, this binding was strengthening by vdW interactions between hydrophobic residues and graphene⁽⁺⁾. In the presence of graphene⁽⁺⁾, the movement of N-terminus was increased over time (Fig. 2a). During simulation, the residues fluctuations reduced over time in the range of 41-91(Gly41-Ser42-Lys43-Thr44-Lys45-Glu46-Gly47-Val48-Val49-His50-Gly51-Val52-Ala53-Thr54-Val55-Ala56-Glu57-Lys58-Thr59-Lys60-Glu61-Gln62-Val63-Thr64-Asn65-Val66-Gly67-Gly68-Ala69-Val70-Val71-Thr72-Gly73-Val74-Thr75-Ala76-Val77-Ala78-Gln79-Lys80-Thr81-Val82-Glu83-Gly84-Ala85-Gly86-Ser87-Ile88-Ala89-Ala90-Ala91). The possible conformational changes occurred following graphene⁽⁺⁾- α -syn interactions may lead to exposing hydrophobic residues in the range of 61-95 (Non-amyloid-beta component (NAC) region). Therefore, it is rational to suggest that vdW interactions occur after initial electrostatic interactions and α -syn structural changes. Thanks to electrostatic interactions between graphene⁽⁺⁾ and α -syn, residues of 39-89 (with overall negative charge) showed highest fluctuations for moving towards positive surfaces during the time of 0-5 ns; (Tyr39-Val40-

Gly41-Ser42-Lys43-Thr44-Lys45-Glu46-Gly47-Val48-Val49-His50-Gly51-Val52-Ala53-Thr54-Val55-Ala56-Glu57-Lys58-Thr59-Lys60-Glu61-Gln62-Val63-Thr64-Asn65-Val66-Gly67-Gly68-Ala69-Val70-Val71-Thr72-Gly73-Val74-Thr75-Ala76-Val77-Ala78-Gln79-Lys80-Thr81-Val82-Glu83-Gly84-Ala85-Gly86-Ser87-Ile88-Ala89) (Fig. 2a). The fluctuations of residues 1-40 increased during their interactions with functional groups of graphene⁽⁺⁾; (Met1-Asp2-Val3-Phe4-Met5-Lys6-Gly7-Leu8-Ser9-Lys10-Ala11-Lys12-Glu13-Gly14-Val15-Val16-Ala17-Ala18-Ala19-Glu20-Lys21-Thr22-Lys23-Gln24-Gly25-Val26-Ala27-Glu28-Ala29-Ala30-Gly31-Lys32-Thr33-Lys34-Glu35-Gly36-Val37-Leu38-Tyr39-Val40). Residues in C-terminus, which have the overall charge of -13 e, showed higher displacements compared to other regions during the time of 0-5 ns and 35-40ns. Our findings show the electrostatic interactions between negative charged residues of α -syn C-terminus and positive functional groups of nano-objects drive α -syn adsorption on the NP surface and hydrophobic forces stabilize these interactions. It is well recognized that short specific amino acid stretches, called hot spot/aggregation prone site, located in NAC region trigger the α -syn fibrillation. Therefore, binding to and blocking this region can be as promising approach for inhibition of α -syn fibrillation process. It can be suggested that graphene⁽⁺⁾ prevent/inhibit α -syn fibrillation through blocking charged residues and hot spot region.

Like graphene⁽⁺⁾, graphene⁽⁻⁾ initially bind to α -syn *via* electrostatic interactions and then hydrophobic forces tighten this binding (Fig. 4a-h). Although the positive charged residues such as Lys trigger the movement of α -syn toward the functional group of graphene⁽⁻⁾, vdW forces stabilize this binding in the end stages of interactions. Moreover, during the interactions of hydrophobic residues with the graphene⁽⁻⁾, the electrostatic interactions between positive charged Lys and functional groups of surface support the vdW energy (Fig. 2a, b). Similarly, the electrostatic interactions between negative charged residues (Glu and Asp) and positive charged graphene⁽⁺⁾ improve the vdW interactions between α -syn and graphene⁽⁺⁾.

As seen in figure 2g, h, the value of RMSF for the C α increased when three α -syn monomers interacted with each other. In contrast, when they interacted with graphene⁽⁺⁾ and graphene⁽⁻⁾, RMSF values and monomer flexibility decreased. In contrast to charged nano-objects, graphene⁽⁰⁾ and SPIONs⁽⁰⁾ showed same RMSF values in the initial and end stages of interactions (0-5 ns and 35-40 ns) (Fig. 2a-g). The stability of NAC region from α -syn monomers exposed to graphene⁽⁺⁾, graphene⁽⁻⁾ and graphene⁽⁰⁾ is different (Fig. 2a-g). Based on RMSF calculations, through interactions of α -syn and graphene⁽⁰⁾, the rigidity of residues 1-32 (Met1-Asp2-Val3-Phe4-Met5-Lys6-Gly7-Leu8-Ser9-Lys10-Ala11-Lys12-Glu13-Gly14-Val15-Val16-Ala17-Ala18-Ala19-Glu20-Lys21-Thr22-Lys23-Gln24-Gly25-Val26-Ala27-Glu28-Ala29-Ala30-Gly31-Lys32), residues 37-45 (Val37-Leu38-Tyr39-Val40-Gly41-Ser42-Lys43-Thr44-Lys45), 57-94 (Glu57-Lys58-Thr59-Lys60-Glu61-Gln62-Val63-Thr64-Asn65-Val66-Gly67-Gly68-Ala69-Val70-Val71-Thr72-Gly73-Val74-Thr75-Ala76-Val77-Ala78-Gln79-Lys80-Thr81-Val82-Glu83-Gly84-Ala85-Gly86-Ser87-Ile88-Ala89-Ala90-Ala91-Thr92-Gly93-Phe94) and residues 116-128 (Met116-Pro117-Val118-Asp119-Pro120-Asp121-Asn122-Glu123-Ala124-Tyr125-Glu126-Met127-Pro128) (Fig. 2e, 5a-h) increased while the rigidity of NAC region decreased. These findings indicate that charged surfaces can be as promising candidates for inhibiting the α -syn fibrillation.

The RMSF values for SPION⁽⁺⁾ are more stable at the end of simulation, rather than initiation stages, in the regions of 1-36 (Met1-Asp2-Val3-Phe4-Met5-Lys6-Gly7-Leu8-Ser9-Lys10-Ala11-Lys12-Glu13-Gly14-Val15-Val16-Ala17-Ala18-Ala19-Glu20-Lys21-Thr22-Lys23-Gln24-Gly25-Val26-Ala27-Glu28-Ala29-Ala30-Gly31-Lys32-Thr33-Lys34-Glu35-Gly36), 42-58 (Ser42-Lys43-Thr44-Lys45-Glu46-Gly47-Val48-Val49-His50-Gly51-Val52-Ala53-Thr54-Val55-Ala56-Glu57-Lys58), 65-75 (Asn65-Val66-Gly67-Gly68-Ala69-Val70-Val71-Thr72-Gly73-Val74-Thr75) and 116-140 (Met116-Pro117-Val118-Asp119-Pro120-Asp121-Asn122-Glu123-Ala124-Tyr125-Glu126-Met127-Pro128-Ser129-Glu130-Glu131-

Gly132-Tyr133-Gln134-Asp135-Tyr136-Glu137-Pro138-Glu139-Ala140) (Fig. 2c). Through SPION⁽⁺⁾- α -syn interactions, the flexibility of residues 37-41 (Val37-Leu38-Tyr39-Val40-Gly41), residues 59-64 (Thr59-Lys60-Glu61-Gln62-Val63-Thr64), 76-99 (Ala76-Val77-Ala78-Gln79-Lys80-Thr81-Val82-Glu83-Gly84-Ala85-Gly86-Ser87-Ile88-Ala89-Ala90-Ala91-Thr92-Gly93-Phe94-Val95-Lys96-Lys97-Asp98-Gln99) and residues 109-115 (Gln109-Glu110-Gly111-Ile112-Leu113-Glu114-Asp115) decreased (Fig. 2c). Moreover, for SPION⁽⁻⁾- α -syn interactions, the rigidity of residues 1-40 (Met1-Asp2-Val3-Phe4-Met5-Lys6-Gly7-Leu8-Ser9-Lys10-Ala11-Lys12-Glu13-Gly14-Val15-Val16-Ala17-Ala18-Ala19-Glu20-Lys21-Thr22-Lys23-Gln24-Gly25-Val26-Ala27-Glu28-Ala29-Ala30-Gly31-Lys32-Thr33-Lys34-Glu35-Gly36-Val37-Leu38-Tyr39-Val40), residues 51-68 (Gly51-Val52-Ala53-Thr54-Val55-Ala56-Glu57-Lys58-Thr59-Lys60-Glu61-Gln62-Val63-Thr64-Asn65-Val66-Gly67-Gly68), residues 71-92 (Val71-Thr72-Gly73-Val74-Thr75-Ala76-Val77-Ala78-Gln79-Lys80-Thr81-Val82-Glu83-Gly84-Ala85-Gly86-Ser87-Ile88-Ala89-Ala90-Ala91-Thr92), residues 97-104 (Lys97-Asp98-Gln99-Leu100-Gly101-Lys102-Asn103-Glu104), residues 112-120 (Ile112-Leu113-Glu114-Asp115-Met116-Pro117-Val118-Asp119-Pro120) and residues 122-127 (Asn122-Glu123-Ala124-Tyr125-Glu126-Met127) increased (Fig. 2d). Indeed, electrostatic interactions between charged residues and negative surface of SPION⁽⁻⁾ trigger α -syn movement toward SPION⁽⁻⁾ and then vdW energy tighten these interactions.

In addition, based on RMSF values it can be suggested that SPION⁽⁺⁾/SPION⁽⁻⁾ bound α -syn show more rigidity than that binds to SPION⁽⁰⁾ (Fig. 2c, d, f). In the case of SPION⁽⁰⁾- α -syn interactions, the flexibility of regions 1-4 (Met1-Asp2-Val3-Phe4), 31-57 (Gly31-Lys32-Thr33-Lys34-Glu35-Gly36-Val37-Leu38-Tyr39-Val40-Gly41-Ser42-Lys43-Thr44-Lys45-Glu46-Gly47-Val48-Val49-His50-Gly51-Val52-Ala53-Thr54-Val55-Ala56-Glu57), 73-81 (Gly73-Val74-Thr75-Ala76-Val77-Ala78-Gln79-Lys80-Thr81), 86-101 (Gly86-Ser87-Ile88-Ala89-Ala90-Ala91-Thr92-Gly93-Phe94-Val95-Lys96-Lys97-Asp98-Gln99-Leu100-

Lys101), 120-123 (Pro120-Asp121-Asn122-Glu123) and 136-140 (Tyr136-Glu137-Pro138-Glu139-Ala140) increased (Fig. 2f, Fig. 8a-h). The significant point about the interactions of charged nano-objects with α -syn is that more residues are involved in the interactions between graphene⁽⁻⁾/graphene⁽⁺⁾ and α -syn compared to SPION⁽⁻⁾/SPION⁽⁺⁾- α -syn interactions (Fig. 3a-h, 4a-h, 6a-h, 7a-h).

We simulated three α -syn monomers to understand the detailed mechanism of α -syn trimmer self-assembly process. The simulations showed that charged residues have most important role in head-to-head interactions of monomers. Furthermore, by calculating RMSF, it was shown that residues in the ranges of 29-41, 43-64, 86-98 and 109-122 have the key roles in triggering α -syn self-assembly process; ((29-41 (Ala29-Ala30-Gly31-Lys32-Thr33-Lys34-Glu35-Gly36-Val37-Leu38-Tyr39-Val40-Gly41), 43-64 (Lys43-Thr44-Lys45-Glu46-Gly47-Val48-Val49-His50-Gly51-Val52-Ala53-Thr54-Val55-Ala56-Glu57-Lys58-Thr59-Lys60-Glu61-Gln62-Val63-Thr64), 86-98 (Gly86-Ser87-Ile88-Ala89-Ala90-Ala91-Thr92-Gly93-Phe94-Val95-Lys96-Lys97-Asp98) and 109-122 (Gln109-Glu110-Gly111-Ile112-Leu113-Glu114-Asp115-Met116-Pro117-Val118-Asp119-Pro120-Asp121-Asn122)). Our findings, confirm the critical role of charged residues in starting/triggering α -syn aggregation. In addition, dipole-monopole and monopole-monopole interactions also contribute in α -syn aggregation. The contribution of these forces is ranked in the following order: dipole-dipole>dipole-monopole>monopole-monopole. Therefore, blocking the charged residues can be as promising therapeutic approach to inhibit/delay α -syn fibrillation. Thanks to their high affinity for charge residues, charged nano-objects can be as the effective therapeutics for inhibiting α -syn fibrillation.

Characterization of functionalized graphene

Graphene derivatives were characterized by various spectroscopy and microscopy methods as well as thermogravimetric and elemental analysis (Fig. 9b-d, tables 1 and 2). According to

transmission electron microscopy (TEM), the average size of large, medium and small graphene sheets was 800-1200 nm, 450-650 nm and 150-250 nm ~~1000 nm, 500-590 nm and 190-210 nm~~ respectively (Fig. 9b). Also thermogravimetric analysis (TGA) showed 70%, 60% and 68% weight loss for graphene sheets with polyglycerolsulfate, polyglycerol and polyglycerolamine coverages (Fig. 9c). Considering the extra weights related to sulfate and amine groups, TGA indicates the same polymer content for different sheets. Graphene sheets with the same functionality but different sizes showed the same surface charges. The surface charges of graphene sheets with polyglycerolsulfate, polyglycerol and polyglycerolamine coverages were around -30 mV (graphene⁽⁻⁾-L: -29±2 mV; graphene⁽⁻⁾-M: -30±1 mV and graphene⁽⁻⁾-S: -31±2 mV), 0 mV (graphene⁽⁰⁾-L: -2±1 mV; graphene⁽⁰⁾-M: -1±1 mV and graphene⁽⁰⁾-S: -1±2 mV), and +30 mV (graphene⁽⁺⁾-L: +32±2 mV; graphene⁽⁺⁾-M: +30±1 mV and graphene⁽⁺⁾-S: +32±1 mV), respectively (See ESI pages 3, 4 and 5).

Materials and methods

Materials

Thermally reduced graphene oxide (TRGO) was provided from Albert-Ludwigs-University Freiburg.¹ Hyperbranched polyglycerol (hPG), with $M_n \approx 10000 \text{ g} \cdot \text{mol}^{-1}$ was synthesized through one-pot, ring-opening anionic polymerization (ROAP).² Sodium azide, triethylamine (TEA), cyanuric chloride, methanesulfonyl chloride, sulfur trioxide pyridine complex, triphenylphosphine (PPh₃), N-methyl-2-pyrrolidone (NMP), N,N-dimethylformamide (DMF), tetrahydrofuran (THF) and ethylenediamine were purchased from Sigma-Aldrich. Milli-Q water was used in all experiments. The 5% amino-functionalized hPG (hPG(NH₂)_{5%}), triazine-functionalized TRGO (TRGO-Trz), hPG conjugated TRGO with different sizes and surface charges were prepared according to our previous publications.^{3, 4}

Density of triazine in TRGO-Trz

Table 1 shows the composition of TRGO and TRGO-Trz based on which the density of triazine

groups could be calculated.

Calculation of triazine density (TD):

$$TD = \frac{\text{number of triazine groups}}{\text{number of carbon atoms of graphene}}$$

Mass of a building block (BB) in TRGO-Trz

$$BB = \frac{100 * 56(\text{Mass of N atoms in one triazine group})}{8.27(\text{percent of N in TRGO - Trz})} = 677.1$$

$$TD = \frac{12(\text{Mass of one carbon atom})}{677.1 - 163.5(\text{Mass of one triazine group})} = 1/42.8$$

Density of hydroxyl groups in Graphene⁽⁰⁾-L, Graphene⁽⁰⁾-M and Graphene⁽⁰⁾-S

According to TGA results, the percent of hPG in Graphene⁽⁰⁾-L, Graphene⁽⁰⁾-M and Graphene⁽⁰⁾-S are around 60%, therefore the percent of graphene backbone is around 40%.

In 1 g Graphene⁽⁰⁾-L, the amount of graphene backbone is 400 mg, meaning 33.3 mmol carbon atoms.

The amount of Trz is $33.3/42.8=0.78$ mmol, meaning 127.5 mg.

The amount of hPG is $1000 - 400 - 127.5 = 472.5$ mg.

The amount of hydroxyl is $472.5/74 = 6.39$ mmol.

Percent of sulfate groups in Graphene⁽⁻⁾-L, Graphene⁽⁻⁾-M and Graphene⁽⁻⁾-S

Calculation of the percent of sulfate groups (PS):

1. Number (NS) and Weight (WS) of sulfate groups in 1 g Graphene⁽⁻⁾-L:

$$\begin{aligned} NS &= \frac{102.5 \text{ mg (weight of sulfur)}}{32 \text{ mg/mmol (molecular mass of sulfur)}} * 1(\text{number of sulfur in one sulfate}) \\ &= 3.2 \text{ mmol} \end{aligned}$$

$$WS = (119 + 57) \text{ mg/mmol} * 3.2 \text{ mmol} = 563.2 \text{ mg}$$

2. Number of hydroxyl groups (NH) in 1 g Graphene⁽⁻⁾-L::

$$NH = \frac{1000 \text{ mg} * 0.7(\text{percent of polymer in Graphene}^{(-)} - L) - 563.2 \text{ mg}}{74(\text{mass of per unit in hPG})} = 1.8 \text{ mmol}$$

$$SP = \frac{NS}{NS + NH} = \frac{3.2 \text{ mmol}}{3.2 \text{ mmol} + 1.8 \text{ mmol}} = 64 \%$$

Percent of amine groups in Graphene⁽⁺⁾-L, Graphene⁽⁺⁾-M and Graphene⁽⁺⁾-S

In the ¹H NMR spectra of mesylated Graphene⁽⁰⁾-L, signal at position 2 (3.4-5.2 ppm) are attributed to the protons of hPG backbone, and the signal at position 1 (3.1-3.3 ppm) correspond to the methyl of methanesulfonyl groups. Based on the peak area ratio of hPG backbone to methanesulfonyl, around 82.3% of the hydroxyl groups on hPG of Graphene⁽⁰⁾-L were mesylated. Therefore, the percent of amine groups in hPG-amino covered TRGO sheets is around 82.3%.

Supplemental Figure Legends

Table S1. The elemental analysis of TRGO and TRGO-Trz.

Table S2. The elemental analysis of graphene⁽⁻⁾-L, graphene⁽⁻⁾-M and graphene⁽⁻⁾-S.

Table S3. List of SPIONs commercially provided from micromod company (Germany).

Figure S1. Molecular structures of six different setups (SPIONs⁽⁰⁾, SPION⁽⁺⁾, SPION⁽⁻⁾, graphenes⁽⁰⁾, graphene⁽⁺⁾, graphene⁽⁻⁾) drawn using V.M.D.1.9.3.

Figure S2. RMSF values for interactions of α -syn with (a) graphene⁽⁺⁾, (b) graphene⁽⁻⁾, (c) SPION⁽⁺⁾, (d) SPION⁽⁻⁾, (e) graphene⁽⁰⁾, (f) SPIONs⁽⁰⁾ and (g) α -syn monomers. (h) Three head-to-head interactions of α -syn during 50 ns.

Figure S3. α -syn binding to graphene⁽⁺⁾. At first, Glu and Asp residues mainly located in C-terminus triggered binding of α -syn to graphene⁽⁺⁾ and then this interaction was tighten by hydrophobic residues such as Val and Ala. The important residues involved in this interactions are Glu139, Glu131, Glu130, Glu105, Asp115, Asp135, Asp98, Glu110, Glu104, Glu132, Glu137, Glu126, Glu46, Glu35, Glu28, Glu20, Glu83, Glu61, Glu57, Ala140, Tyr136, Gln99, Tyr125, Leu113, Ile112, Pro108 and Gln107.

Figure S4. α -syn binding to graphene⁽⁻⁾. At first, Lys residues in N-terminus induce the movement of α -syn toward graphene⁽⁻⁾ and then hydrophobic residues such as Val, Tyr and Ala support this binding. The important residues involved in these interactions are Lys58, Thr59, Lys60, Lys80, Lys96, Lys97, Lys106, Lys102, Lys32, Lys23, Lys21, Lys6, Lys10, Lys12, Glu139, Glu131, Glu130, Glu105, Asp121, Asp98, Glu110, Gly106, Gly101, Glu132, Pro138, Ala140, Tyr 136, Gln107, Tyr133, Leu 113, Ile 112, Pro108, Lys34, Lys43 and Gln107.

Figure S5. Interactions between graphene⁽⁰⁾ and α -syn. The charged residues in N-terminus and C-terminus are not involved in these interactions. The vdW force drives strong interactions between central region of α -syn and graphene⁽⁰⁾.

Figure S6. α -syn binding to SPION⁽⁺⁾. At first, Asp, Ala and Val residues mediate binding of α -syn to SPION⁽⁺⁾ and then hydrophobic residues such as Val and Ala strengthen this binding.

The critical residues involved in these interactions are Glu139, Glu131, Glu130, Glu105, Asp115, Asp135, Asp98, Glu110, Glu104, Glu132, Glu137, Glu126, Glu123, Glu126, Glu137, Glu13, Glu20, Glu28, Glu35, Glu46, Glu57, Glu61, Glu83.

Figure S7. α -syn binding to SPION⁽⁻⁾. At first, Val and Lys residues located at N-terminus trigger the binding of α -syn to SPION⁽⁻⁾. After attachment of α -syn to SPION⁽⁻⁾, hydrophobic residues such as Val and Ala support this attachment and then Lys43, Lys102, Lys97, Lys96, Gln99, Glu139, Phe4, Gln114, Pro108, Lys80, Lys6, Lys10, Lys12, Lys21, Lys23, Lys32, Lys34, Lys58, Lys60 are involved.

Figure S8. Interactions between SPION⁽⁰⁾ and α -syn. The charged residues in N-terminus and C-terminus and electrostatic force are not involved in these interactions. vdW force leads to weak interactions between central region (NAC region) of α -syn and SPION⁽⁰⁾.

Figure S9. (a) Graphene derivatives with similar polymer coverage but different surface charges and sizes. * denotes tip sonication for 15 min; (b) TGA diagrams of graphene derivatives, showing similar polymer content for these compounds. Polyglycerol, polyglycerolsulfate and polyglycerolamine coverages were decomposed at 200-400 °C, 200-700 °C and 250-400 °C, respectively. (c) TEM images and size distributions of graphene derivatives with different surface charges and sizes (Scale bar: 1000 nm). (d) ¹H NMR spectrum of mesylated graphene⁽⁰⁾-L.

Figure S10. Effect of (a, b) SPIONs⁽⁰⁾ with different sizes (50, 100 nm) on the α -syn fibrillation monitored by ThT fluorescence. Kinetic parameters ((c) relative half time ($t_{1/2}/t_{1/2, \text{control}}$), (d) relative ThT end level, (e) relative lag time ($t_N/t_{N, \text{control}}$) and (f) relative growth rate (v/v_{control})) for α -syn fibrillation as a function of various concentration of SPIONs⁽⁰⁾ with different sizes relative to the values in the absence of the SPION⁽⁰⁾. Effect of (g-l) graphenes⁽⁰⁾/graphene⁽⁻⁾/graphene⁽⁺⁾ with different sizes (200, 500, 1000 nm) on the α -syn fibrillation monitored by ThT fluorescence. Kinetic parameters ((m, p, u) relative half time ($t_{1/2}/t_{1/2, \text{control}}$), (n, r, v) relative ThT end level, (o, s, w) relative lag time ($t_N/t_{N, \text{control}}$) and (p, t, x) relative growth rate (v/v_{control})) for α -syn fibrillation as a function of various concentration of graphenes⁽⁰⁾/graphene⁽⁻⁾/graphene⁽⁺⁾ with different sizes relative to the values in the absence of the graphenes⁽⁰⁾/graphene⁽⁻⁾/graphene⁽⁺⁾.

Table 1S

Elemental Analysis	N (%)	C (%)	H (%)	S (%)
TRGO	0.036	81.54	1.322	0
TRGO-Trz	8.27	77.62	2.163	0

Table 2S

Elemental Analysis	C (%)	H (%)	N (%)	S (%)
Graphene ⁽⁻⁾ -L	32.23	4.16	2.42	10.25
Graphene ⁽⁻⁾ -M	33.37	4.54	2.29	10.57
Graphene ⁽⁻⁾ -S	33.19	4.27	2.37	10.44

Table 3S

Nanoparticle	Size	Surface modification	Prod. code	Company
nanomag®-D-spio	20 nm	Plain	79-00-201	Micromod
nanomag®-D-spio	50 nm	Plain	79-00-501	Micromod
nanomag®-D-spio	100 nm	Plain	79-00-102	Micromod
nanomag®-D-spio	20 nm	NH ₂	79-01-201	Micromod
nanomag®-D-spio	20 nm	COOH	79-02-201	Micromod
nanomag®-D-spio	20 nm	PEG3000	79-54-201	Micromod
nanomag®-C	150 nm	Chitosan	04-00-152	Micromod

Figure S1

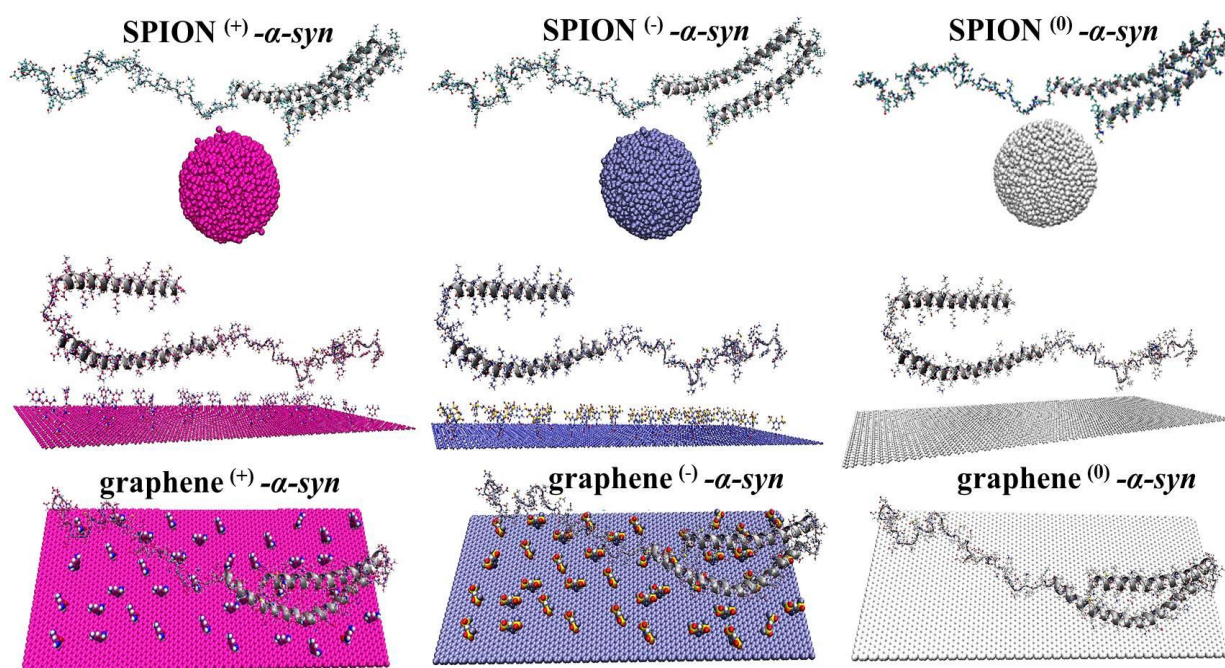


Figure S2

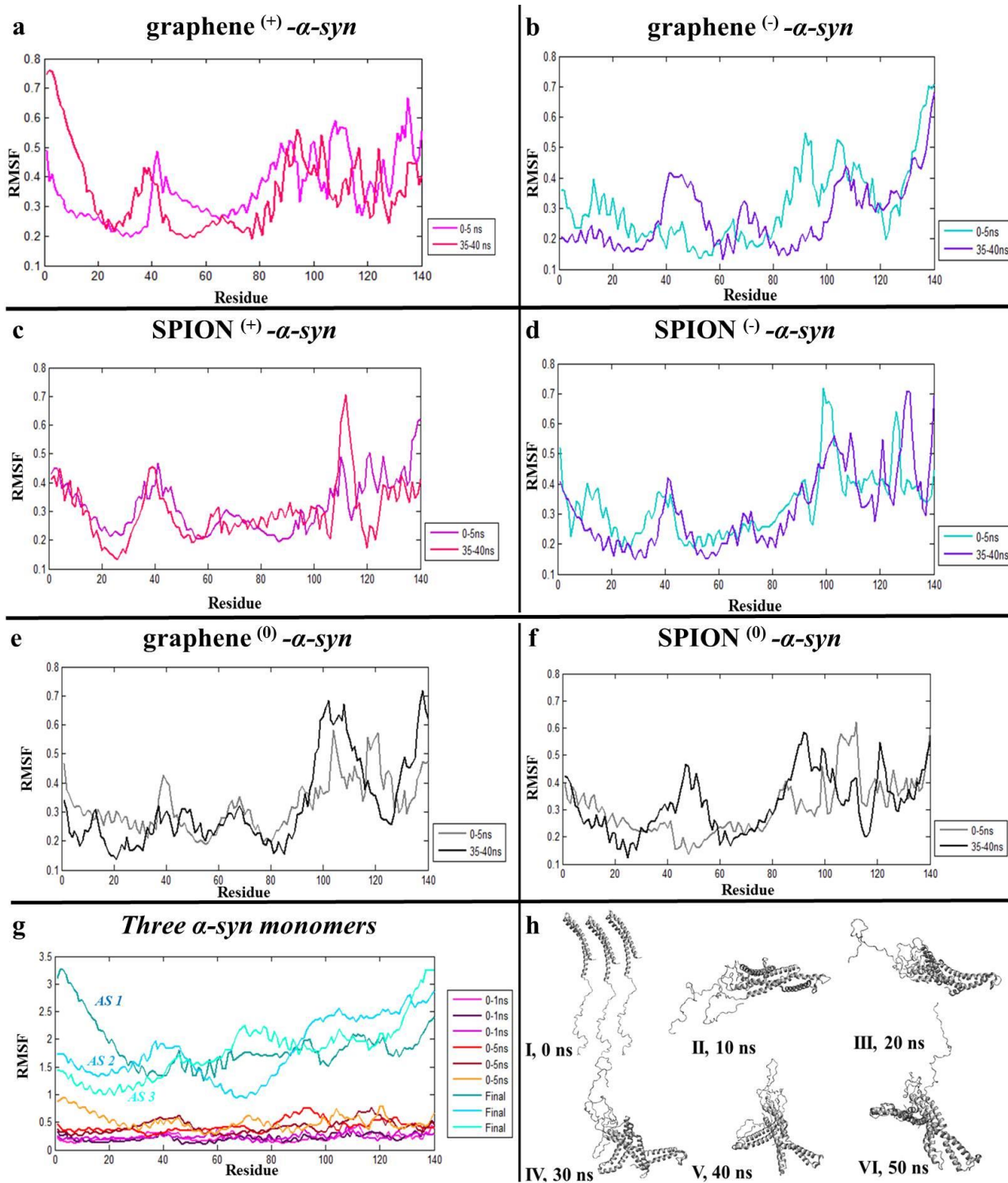


Figure S3

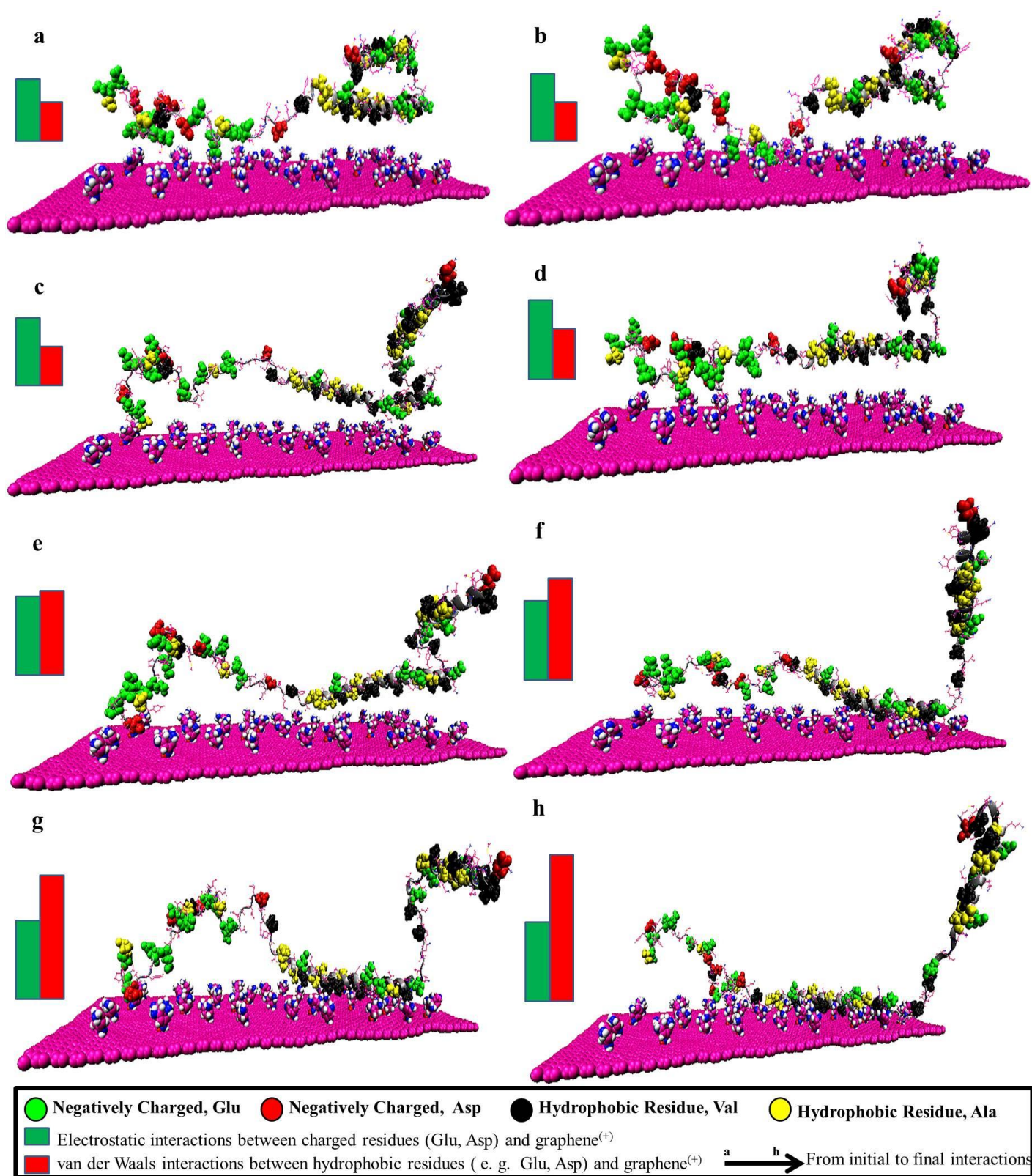


Figure S4

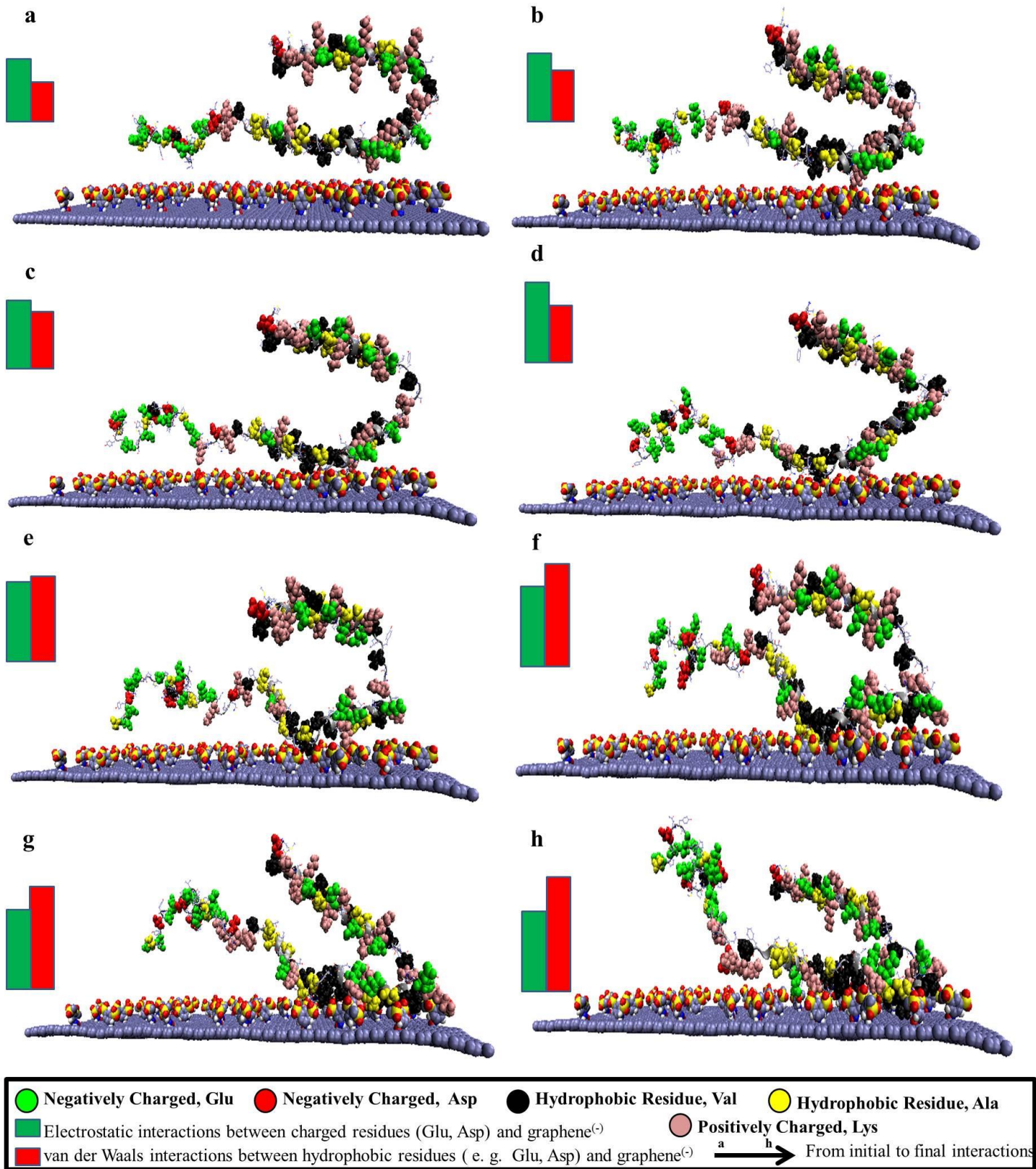


Figure S5

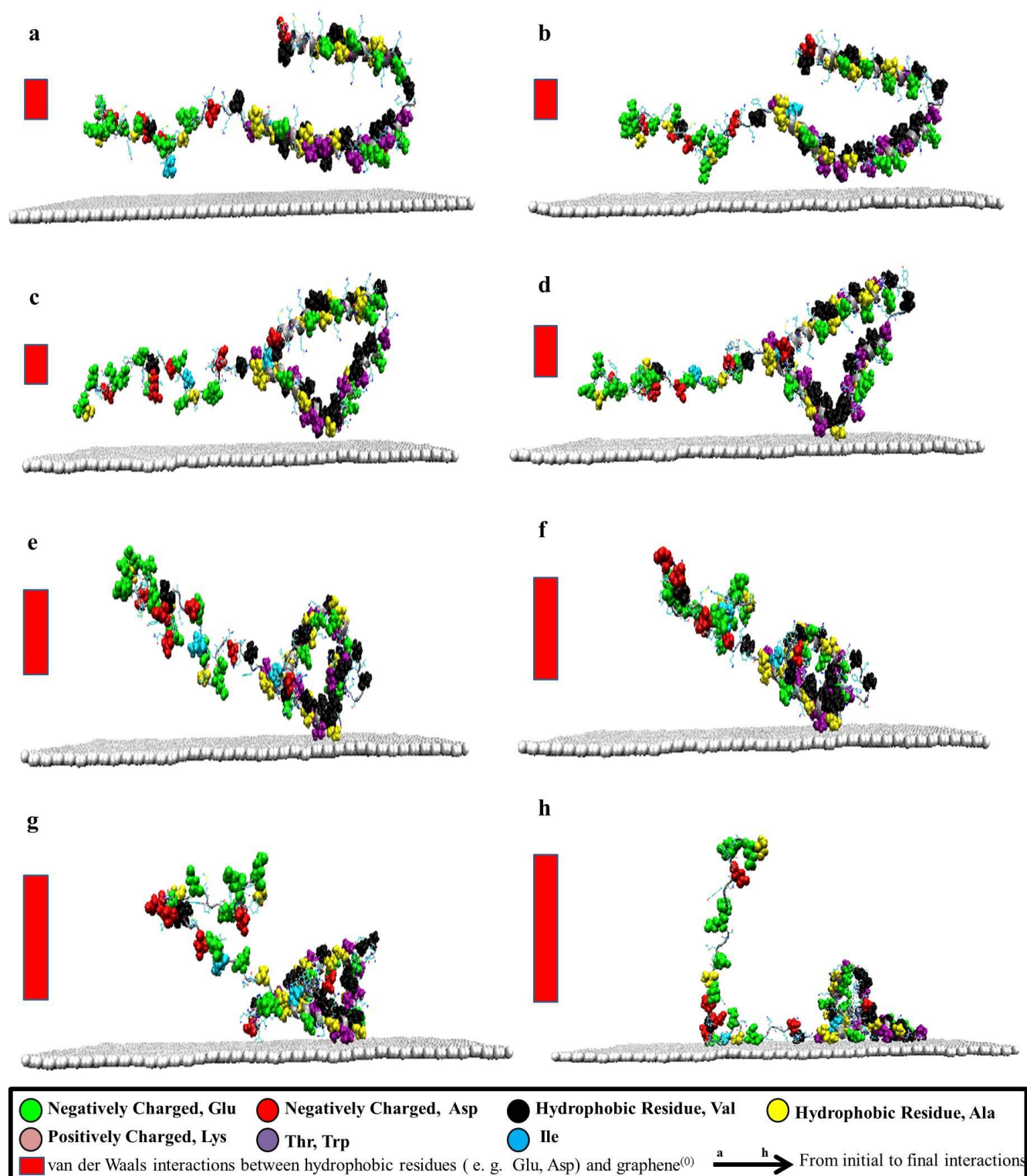


Figure S6

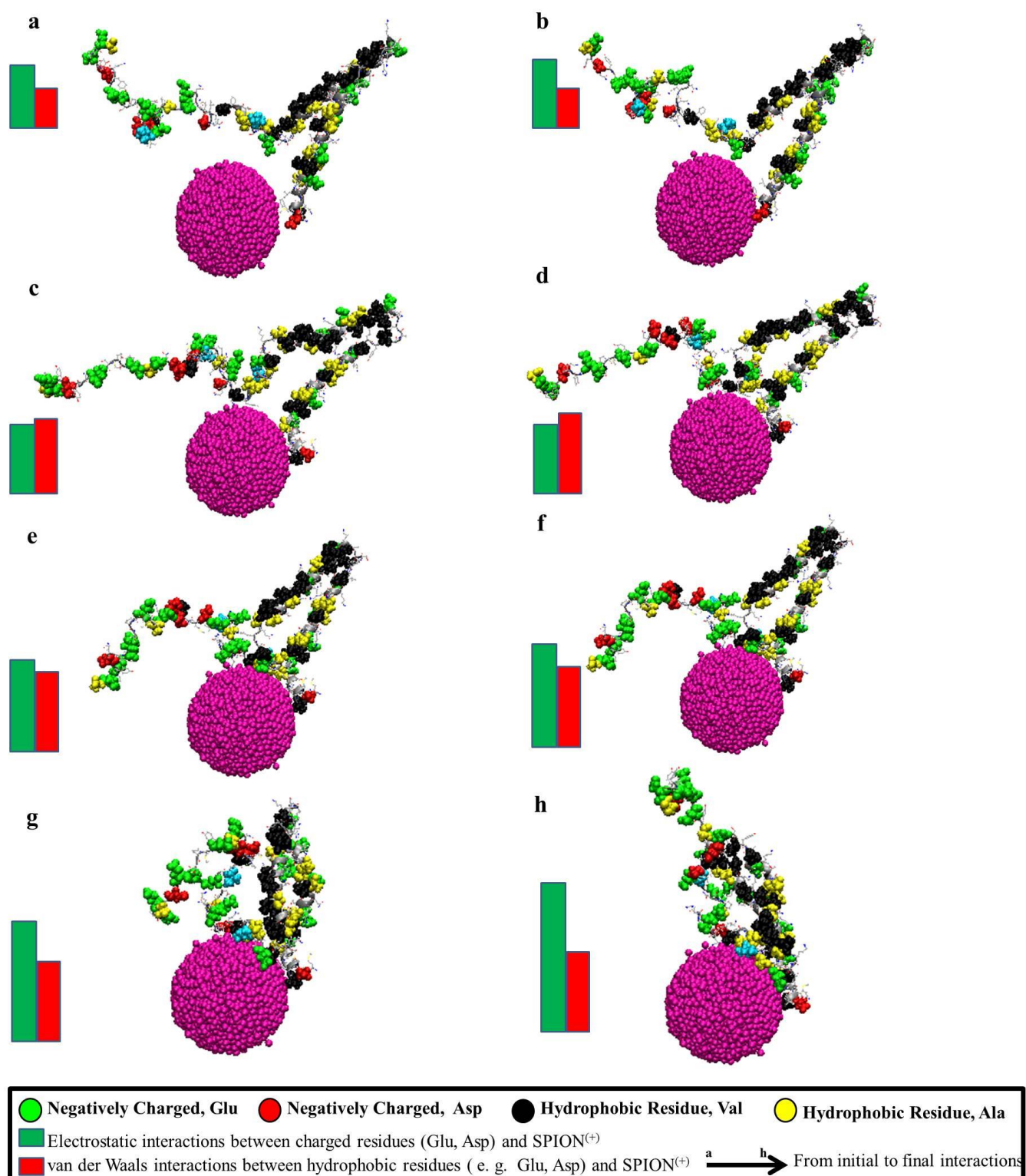


Figure S7

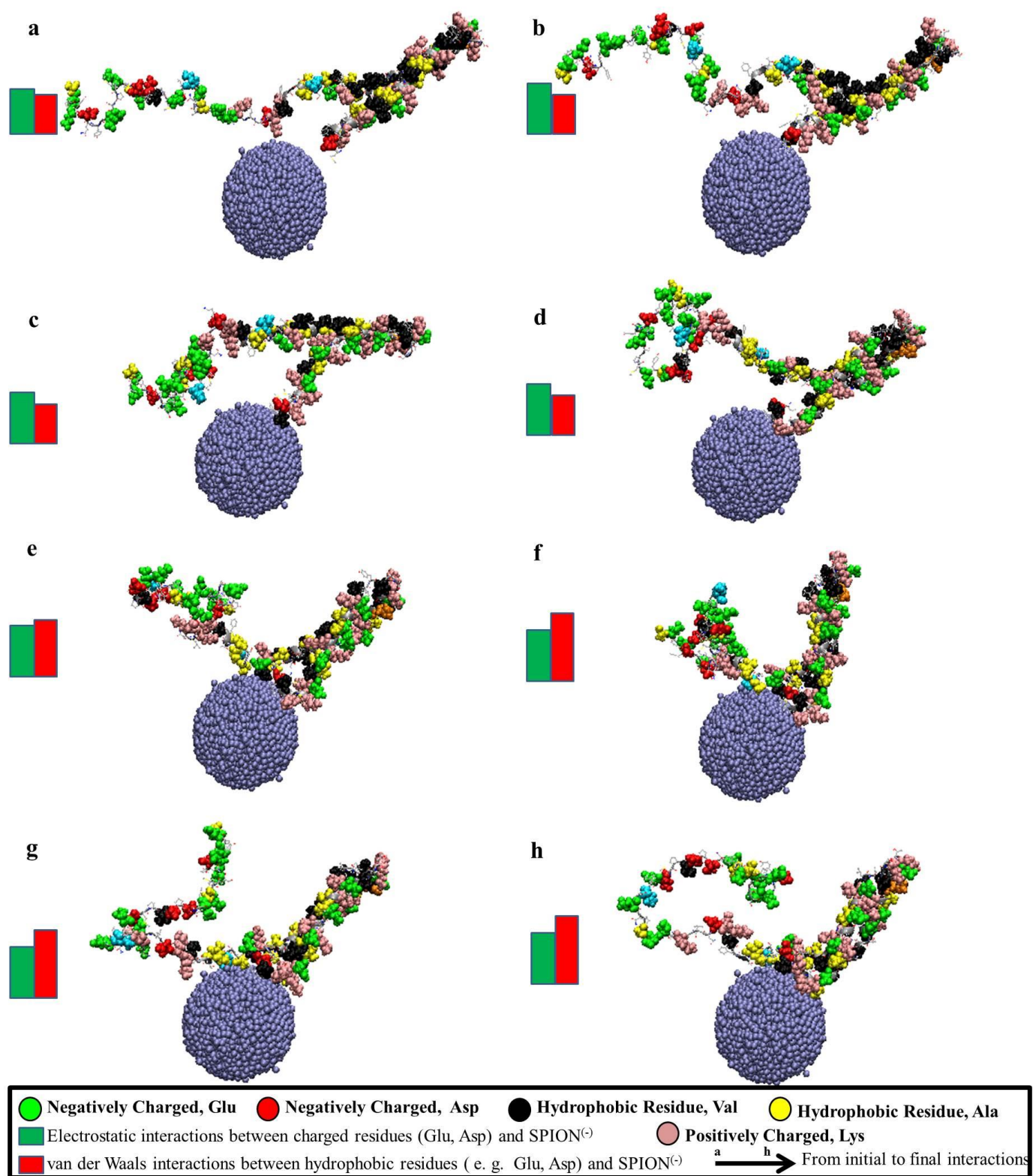


Figure S8

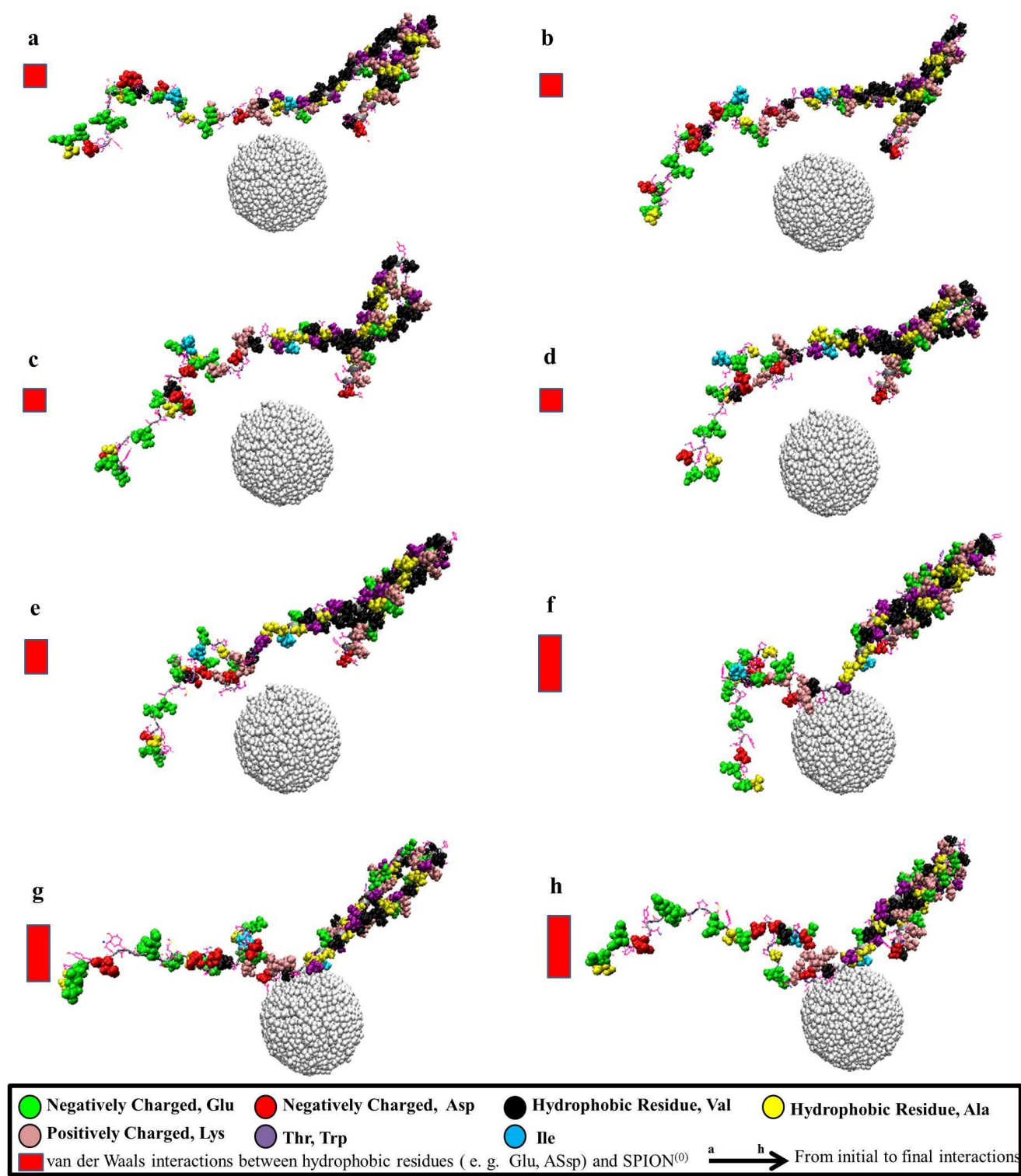


Figure S9

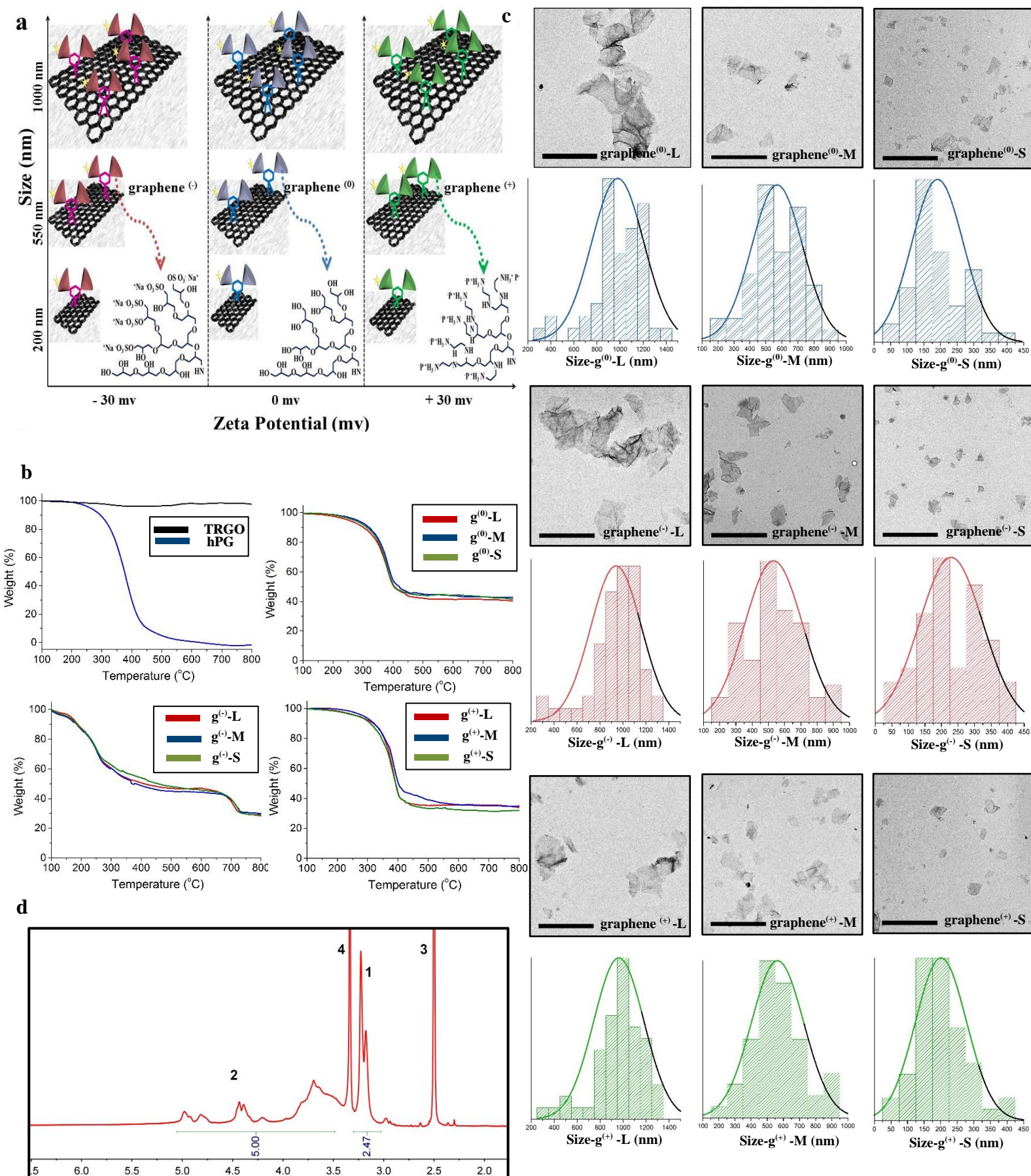
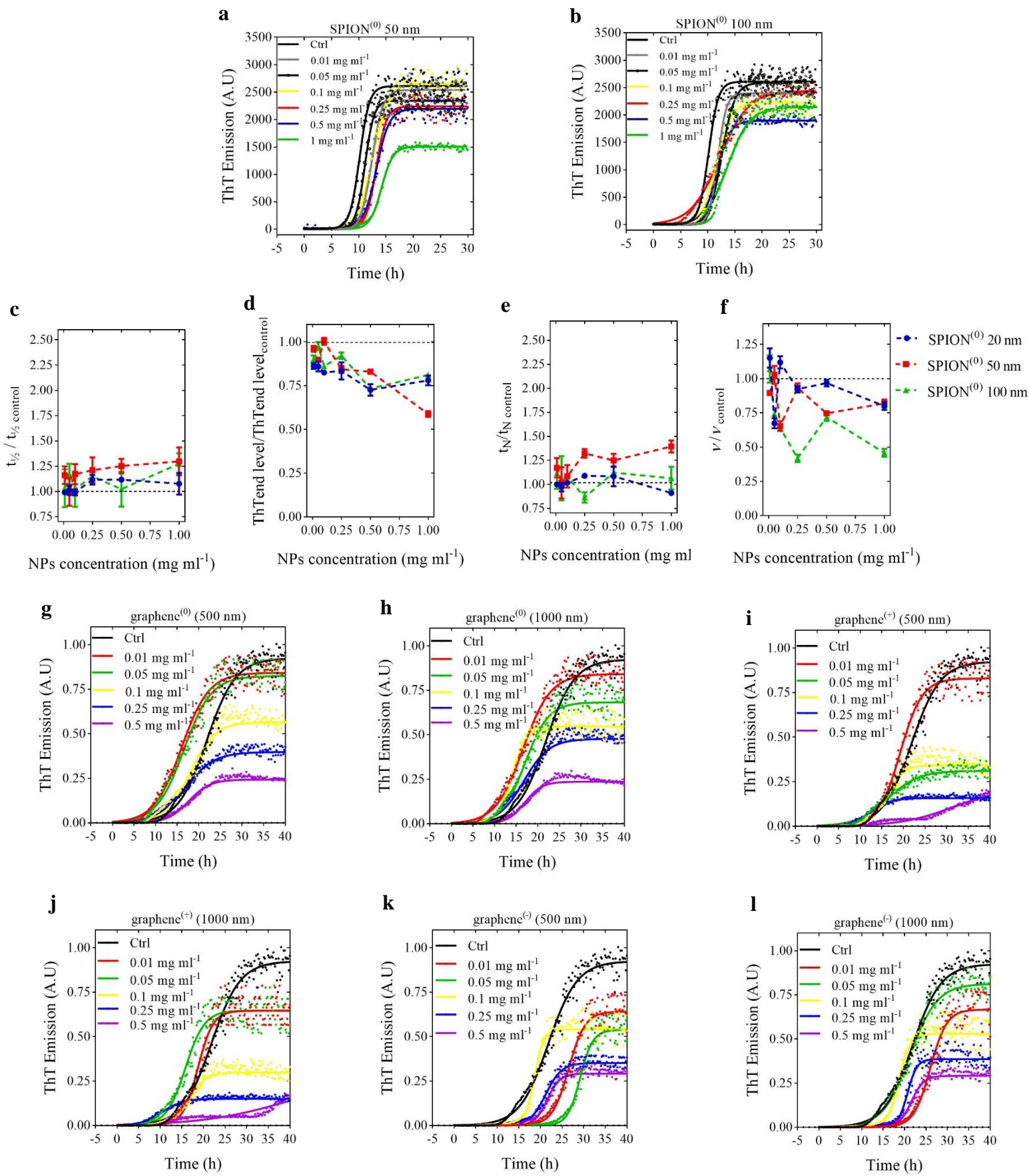
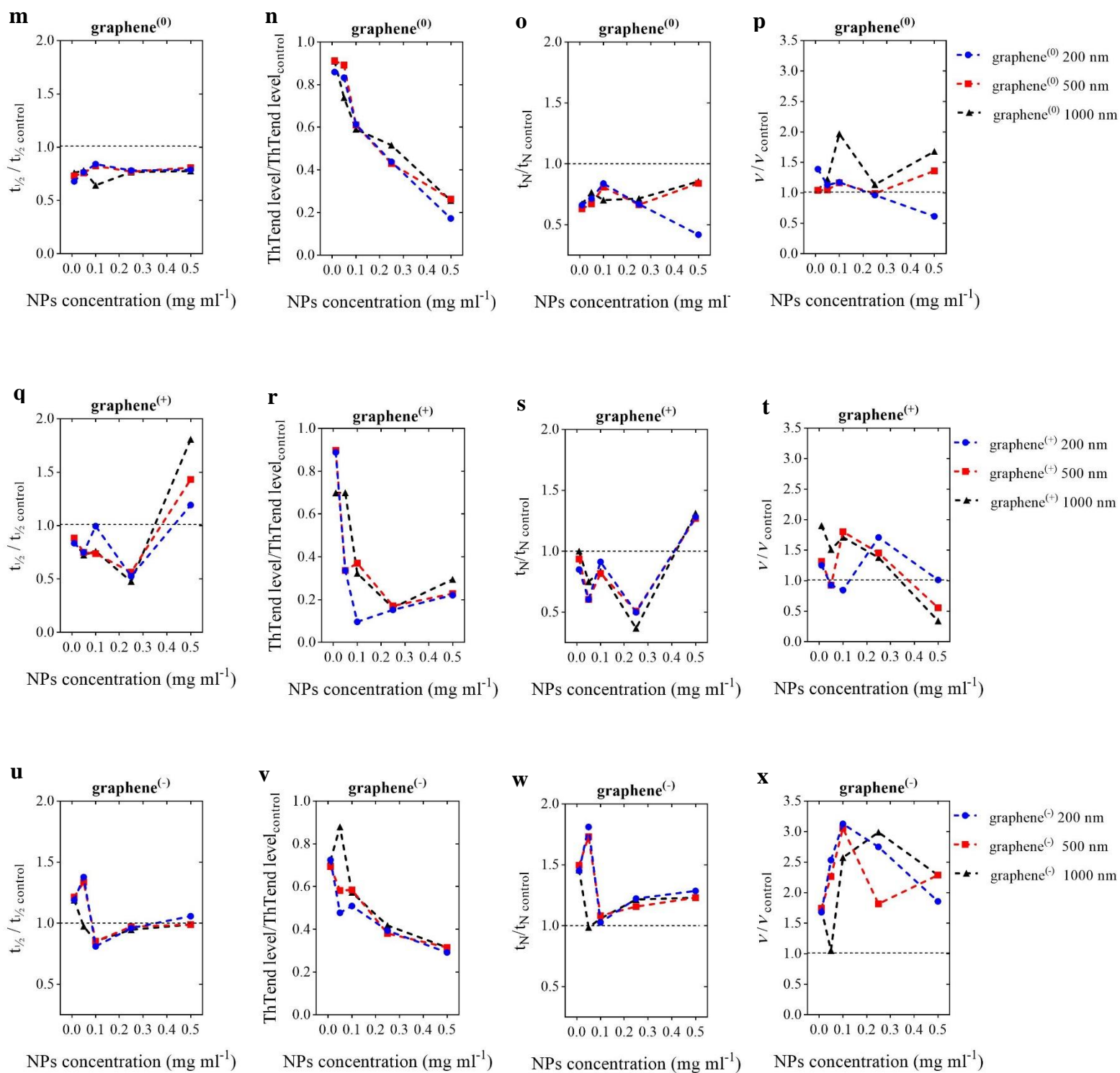


Figure S10





References

1. Schlüter, B.; Mülhaupt, R.; Kailer, A. Synthesis and Tribological Characterization of Stable Dispersions of Thermally Reduced Graphite Oxide. *Tribol Lett.* **2014**, *53*, 353-363.
2. Calderón, M.; Quadir, M. A.; Sharma, S. K.; Haag, R. Dendritic Polyglycerols for Biomedical Applications. *Adv. Mater.* **2010**, *22*, 190-218.
3. Tu, Z.; Achazi, K.; Schulz, A.; Mülhaupt, R.; Thierbach, S.; Rühl, E.; Adeli, M.; Haag, R. Combination of Surface Charge and Size Controls the Cellular Uptake of Functionalized Graphene Sheets. *Adv. Funct. Mater.* **2017**, *27*, 1701837.
4. Tu, Z.; Wycisk, V.; Cheng, C.; Chen, W.; Adeli, M.; Haag, R. Functionalized Graphene Sheets for Intracellular Controlled Release of Therapeutic Agents. *Nanoscale* **2017**, *9*, 18931-18939.